Bioengineering Bacterial Cellulose/Poly(ethylene oxide) Nanocomposites

Elvie E. Brown and Marie-Pierre G. Laborie*

Wood Materials and Engineering Laboratory, Washington State University, P.O. Box 641806, Pullman, Washington 99164-1806

Received April 24, 2007; Revised Manuscript Received July 13, 2007

By adding poly(ethylene oxide) (PEO) to the growth medium of *Acetobacter xylinum*, finely dispersed bacterial cellulose (BC)/PEO nanocomposites were produced in a wide range of compositions and morphologies. As the BC/PEO w/w ratio increased from 15:85 to 59:41, the cellulose nanofibers became smaller but aggregated in larger bundles, indicating that PEO mixed with the cellulose on the nanometer scale. Fourier transform infrared spectroscopy suggested intermolecular hydrogen bonding and also preferred crystallization into cellulose I_β in the BC/PEO nanocomposites. The fine dispersion of cellulose nanofibers hindered the crystallization of PEO, lowering its melting point and crystallinity in the nanocomposites although remaining bacterial cell debris also contributed to the melting point depression. The decomposition temperature of PEO also increased by approximately 15 °C, and the tensile storage modulus of PEO improved significantly especially above 50 °C in the nanocomposites. It is argued that this integrated manufacturing approach to fiber-reinforced thermoplastic nanocomposites affords a good flexibility for tailoring morphology and properties. These results further pose the question of the necessity to remove bacterial cells to achieve desirable materials properties in biologically derived products.

Introduction

Bacterial cellulose (BC) has long been used in a variety of applications in the paper, food, and electronic industries.[1−5] Owing to its high porosity, water absorbance, mechanical properties, formability, and biocompatibility, bacterial cellulose has also recently attracted a great deal of attention for biomedical applications.[6] For instance, bacterial cellulose has been successfully used for wound dressings.[7−9] and for vascular implants.[10,11] The potential of BC for in vitro and in vivo tissue regeneration also continues to be explored and shows great promise.[12−15]

For such biomedical applications it is highly desirable to fine-tune the properties of the scaffold or implant to match the properties of the material that it intends to regenerate or replace.[16] To that end researchers have engaged in augmenting bacterial cellulose. For instance, bacterial cellulose has been soaked into hydroxyapatite to develop a composite scaffold for bone regeneration.[17,18] Bacterial cellulose has also been augmented by immersion in solutions of polyacrylamide and gelatin, yielding hydrogels with improved toughness.[19] Similarly, immersion of bacterial cellulose into poly(vinyl alcohol) has yielded hydrogels having a wide range of mechanical properties of interest for cardiovascular implants.[20]

Another means of altering the properties of bacterial cellulose has been to manipulate its biosynthesis so as to synthesize copolymers or miscible blends. Ciechanska[21] produced bacterial cellulose in a chitosan-enriched medium, thus developing BC/chitosan copolymers with improved water absorbance and mechanical properties. Seifert et al.[22] added cellulose derivatives and poly(vinyl alcohol) in the culture medium, yielding a composite material with improved water retention ability and ion absorption.

The latter synthetic approach, in which bacterial cellulose is modified with a host polymer during biosynthesis, is particularly interesting because competitive adsorption of the host polymer present in the culture medium can alter the crystallization of cellulose, affording a range of morphologies.[23−26] In the case of *Acetobacter xylinum*, glucan chain sheets are extruded from the membrane enzymatic terminal complexes[27] into the aqueous medium where they crystallize into 3−7-nm-wide microfibrils of cellulose I_α primarily, which then aggregate into twisting ribbons with cross-sections of 3−4 nm × 70−140 nm.[27−30] When a compatible polymer is present in the culture medium, competitive adsorption of the host polymer onto the glucan chains hinders the crystallization into microfibrils and ribbons resulting in smaller crystalline structures.[23] Many studies have considered cellulose derivatives, hemicelluloses, and pectins with a view to shedding light on the biogenesis of cellulose and plant cell walls.[23−26] As expected, the compatibility between the polymer and the cellulose governs the alterations that take place in the cellulose in terms of microfibril and ribbon dimensions, crystalline allomorphs, and crystallinity index.[23−26]

It is therefore clear that fiber morphology can be tailored by adding a water-soluble polymer in the culture. In particular, this biotechnological tool could be used for developing bacterial cellulose reinforced thermoplastic nanocomposites in which composition and morphology may be tailored to yield desirable properties for a specific application. In this scenario, the selection of the thermoplastic polymer and its content in the culture can be predicted to govern the nanocomposite morphology and composition. Yet this potential to simultaneously tailor cellulose morphology and its dispersion into a thermoplastic polymer matrix for the manufacture of nanocomposites with improved properties has not been exploited. This research aims at demonstrating that by modifying the culture conditions of bacterial cellulose with a thermoplastic polymer, poly(ethylene oxide) (PEO), nanocomposites can be synthesized with a range of compositions and morphologies. PEO is of particular interest

* Author to whom correspondence should be addressed. Phone: (509) 335-8722. Fax: (509) 335-5077. E-mail: mlaborie@wsu.edu.

10.1021/bm700448x CCC: $37.00
Published on Web 09/01/2007

as it is biocompatible, water-soluble, and therefore widely used in biomedicine.[31] Furthermore, the possibility for hydrogen bonding between the PEO ether oxygen and the cellulose C_6 hydroxyl[32−34] suggests that PEO may be efficient at altering the crystallization of cellulose, yielding a range of fiber and nanocomposite morphologies. By tailoring the composition and morphology of the BC/PEO nanocomposites, it is further hypothesized that physical, thermal, and mechanical properties can be fine-tuned. This goal is of significance not only for improved utilization of bacterial cellulose in various applications but also as a demonstration of how biotechnology and nanotechnology may be combined to design the morphology and properties of nanocomposites. To our knowledge, the potential to simultaneously tailor cellulose morphology and its dispersion in a thermoplastic polymer matrix for the manufacture of nanocomposites with improved thermal and mechanical properties has not been exploited to date.

Materials and Methods

Production of the Starter Culture. *Acetobacter xylinum* of the strain 23769 was purchased from the American Type Culture Collection and maintained in Hestrin−Schramm (HS) medium with a pH adjusted to 5.0 with hydrochloric acid.[35] Specifically, the medium was first autoclaved at 121 °C for 15 min and then inoculated with the bacterial strain and cultivated in static conditions at 29 ± 1 °C in an incubator. After 1 week of production, a gelatinous pellicle had developed at the air/liquid interface. The gelatinous pellicle was removed and pressed to release the cells into the remaining medium, which was used as the inoculum for producing the BC/PEO materials as detailed next.

Production of Bacterial Cellulose in PEO-Modified Media. Poly(ethylene oxide) ($M_w = 1 \times 10^5$ g/mol) from Fisher Scientific was added to a 250 mL Erlenmeyer flask containing 150 mL of HS medium to produce five different culture media with PEO concentrations of 0.5%, 1%, 2%, 3%, and 5% w/w. The different PEO concentrations were expected to lead to nanocomposites with distinct PEO contents. The PEO-modified culture media were inoculated with 20 mL of the inoculum, and after 2 days of cultivation in static conditions at room temperature under a laminar flow hood, the gelatinous pellicle that developed at the air/liquid interface was removed. The remaining medium was further cultivated under the same conditions but under magnetic stirring at ca. 500 rpm. Under agitated conditions, strings of materials started appearing on the second day of growth, and they were collected on the seventh day by filtering with gauze. The collected material, approximately 3 g, was then washed with 250 mL aliquots of distilled water under gentle stirring to eliminate the culture medium and byproducts. This washing procedure was repeated up to 10 times until disappearance of the yellow color from the peptone and yeast extract. Some of the PEO material was also likely lost during the washing procedure. No procedure was undertaken to remove the bacterial cells that remained as whole cells for all characterizations except in the thermal analyses where the high temperatures lysed the cells. The washed samples were then characterized by Fourier transform infrared spectroscopy (FTIR), atomic force microscopy (AFM), and various thermal analyses. For FTIR transparent films were produced by flattening a few milligrams of the washed material into 3×3 cm^2 plastic bags and then freeze-drying. For the thermal analyses 7×3.3 cm^2 films were compression-molded to a thickness of 1.0 ± 0.4 mm using a hydraulic press operating at room temperature under 4000 psi. All products were kept in vacuum desiccators with anhydrous calcium sulfate until characterization. Some of the fresh material was prepared for transmission electron microscopy (TEM) by mounting a drop of wet sample on unsupported 400 mesh copper TEM grids. The grids were also lightly washed with distilled water to remove the low molecular weight contaminants from the culture medium.

Three batches of BC/PEO products were grown for each media, yielding triplicate samples for each characterization technique. Furthermore, weights were recorded at all stages of the sample preparation. Control PEO samples were also prepared by placing PEO into an aqueous solution and following the same sample preparation as that for the BC/PEO products.

Transmission Electron Microscopy. The loaded TEM grids were air-dried and negatively stained with 1% uranyl acetate. TEM images were acquired at 60 000K and at 100 000 magnifications on a JEOL 1200 EX operating at 100 kV. Microfibril dimensions were computed from 8−15 measurements.

Atomic Force Microscopy. A $5 \times 3 \times 0.6$ mm^3 sample was retrieved from the compression-molded product and bonded to the AFM sample disk. The sample surface was trimmed with a glass knife mounted on a cryogenic ultra-microtome (PowerTome-X, RMC Products). Imaging was then performed in tapping mode on a Veeco Multimode atomic force microscope equipped with a NanoScope IIIa controller. A silicon cantilever having a resonance frequency around 200−300 kHz and a nominal spring constant of 40 N/m was used along with a 3×3 μm^2 J-scanner. The scan rate was 1.5 Hz, and integral and proportional gains were 0.3 and 0.5, respectively. Twenty measurements of the observed structures were taken from samples prepared from distinct batches.

Thermogravimetric Analysis. To determine composition and thermal stability, control PEO, pure BC, and the composite products were characterized in accordance with ASTM E 1131[36] on a Rheometrics STA 625. Approximately 10−25 mg of powder material was retrieved from the compression-molded products and placed in aluminum pans in the thermogravimetric analyzer operating under 90 mL/min N_2 flow. After equilibration at 30 °C for 5 min, the sample was heated to 600 °C at 20 °C/min at which point only ashes remained. Raw and derivative weight data were used to determine decomposition temperatures and the associated weight losses. Triplicate measurements were performed.

Fourier Transform Infrared Spectroscopy. FTIR spectra of the neat components and the BC/PEO products were obtained in transmission mode on a Nicolet Nexus 670 Fourier transform infrared spectrometer. While the freeze-dried cellulose and BC/PEO products could be analyzed as thin films, the control PEO required pressing into KBr pellets. Forty scans were acquired in the 4000−600 cm^{-1} range with a resolution of 4 cm^{-1}. Samples were analyzed in duplicate.

Differential Scanning Calorimetry. Approximately 11 ± 4 mg of powder material from the compression-molded products was loaded into aluminum pans and placed in a Mettler Toledo DSC 822e. All differential scanning calorimetry (DSC) experiments were conducted under a N_2 flow of 80 mL/min and controlled cooling with liquid N_2. A temperature program was conducted to record the glass transition temperature (T_g), melting temperature (T_m), and heat of fusion (ΔH_f) of the PEO. Namely, the samples were heated to 100 °C at 20 °C/min and kept at that temperature for 5 min to erase thermal histories, after which they were cooled down to −100 °C at a cooling rate of 30 °C/min. A second heating scan was then conducted from −100 to 100 °C at 20 °C/min, and thermal transitions were recorded.

Dynamic Mechanical Analysis. The compression-molded samples were cut into strips of approximate dimensions of $34 \times 7 \times 0.6$ mm^3 and tested in tension mode on a Rheometrics RSA II. The thermal history of the samples was first erased by heating to 100 °C, except for the control PEO that was heated to 55 °C only. The samples were then cooled to 30 °C, and a dynamic strain sweep was performed at 1 Hz to determine the linear viscoelastic range. The samples were further cooled (30 °C/min) to −70 °C. Using a dynamic strain level lower than 4×10^{-4} within the linear viscoelatic range and a frequency of 1 Hz, a temperature scan was then conducted at 2 °C/min to 100 °C. Duplicate measurements were performed.

Results and Discussion

Morphology of Cellulose/PEO Nanocomposites. The modification of the HS medium with a host polymer capable of

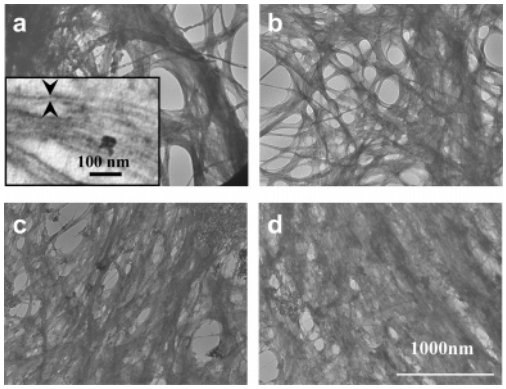

Figure 1. TEM images (60 000) of BC/PEO products: BC grown in (a) HS medium, (b) HS medium with 1% PEO, (c) HS medium with 3% PEO, and (d) HS medium with 5% PEO. The inset in part a illustrates the measurement of nanofiber width at 100 000 magnification images.

interacting with cellulose is expected to alter the aggregation and crystallization of glucan chains into cellulose microfibrils and ribbons, possibly resulting in smaller and more dispersed structures.[23−26] To evaluate the effects of PEO on cellulose crystallization, TEM images of the products retrieved from the standard HS medium and from the HS medium modified with 1%, 3%, and 5% PEO were captured at 60 000 and 100 000 magnifications. Representative images for these magnifications are shown in Figure 1. When grown in the standard HS medium, the smallest observable cellulose structures that formed from *Acetobacter xylinum* were 17 ± 5 nm in width, slightly larger than the microfibrils that are generally observed under static conditions.[30,37] These structures are referred to as nanofibers in this paper. As PEO was added to the HS medium, two changes in the structure and morphology of BC were apparent from the TEM images (Figure 1). First, the nanofibers became smaller, with widths of ca. 10 nm with 1% or more PEO addition. Concomitantly, the cellulose and PEO aggregated to the point that the nanofibers could only be distinguished in a few locations of the micrographs when grown in a 5% PEO content HS medium. The fading away of the nanofiber contours was likely due to the entrapment of the uranyl acetate in the cellulose and PEO aggregates, thus impeding contrast.

While TEM provided information on the in vivo crystallization of cellulose, nanofiber dispersion in the PEO matrix was further visualized on the compression-molded samples with AFM (Figure 2). Recall however that for the AFM images the samples were highly processed as they were compression-molded. Samples changed from having a fibrous and rough surface for neat BC to having a smoother surface in the BC/PEO products thereby facilitating AFM imaging. The smallest structures that could be distinguished with AFM in the neat BC samples were bundles of nanofibers with widths in the 75−111 nm range. As the PEO concentration in the culture medium increased, the bundles of nanofibers also grew wider, reaching sizes in the 121−770 nm range at 5% PEO addition in the culture medium, indicating that nanofibers were bonded together by PEO (Table 2).

The morphological changes observed with TEM and AFM corroborate the proposition that by adding PEO into the HS

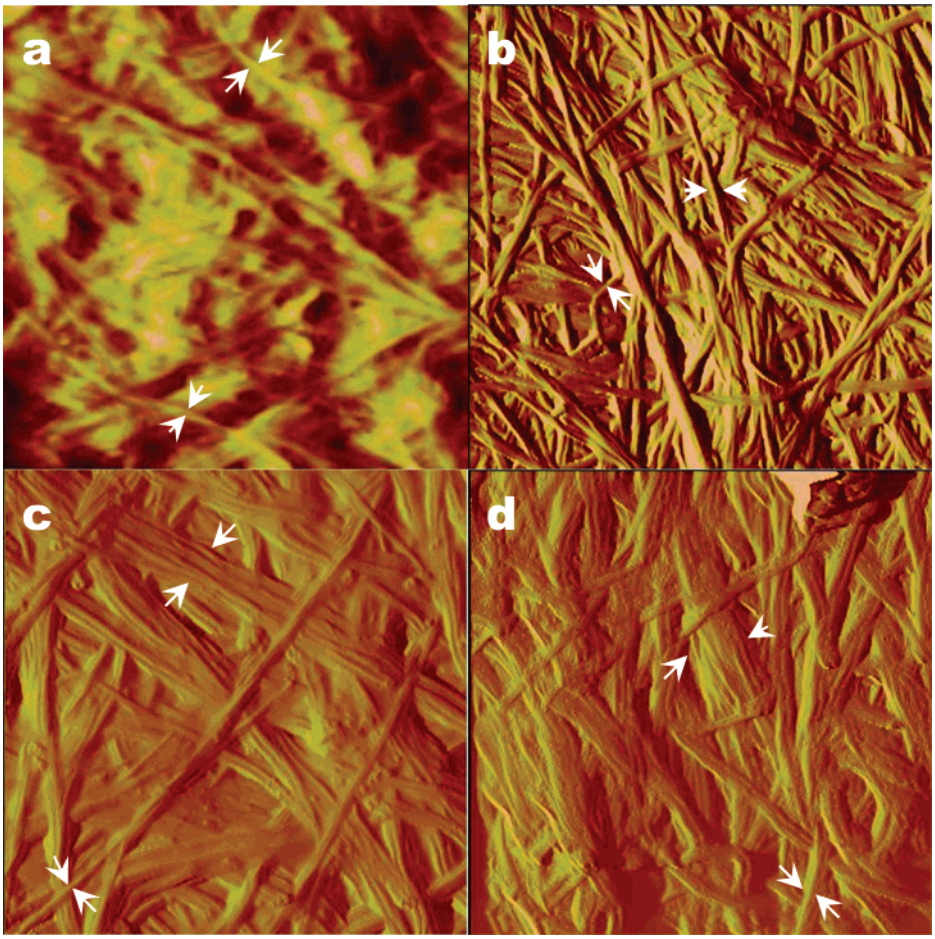

Figure 2. AFM topographical images (3 × 3 μm^2) of BC/PEO products obtained in (a) HS medium, (b) HS medium with 1% PEO, (c) HS medium with 3% PEO, and (d) HS medium with 5% PEO. (Arrows indicate measurements of nanofiber bundles.)

Table 1. Degradation Temperature and Composition of BC and PEO and Their Nanocomposites

	degradation temperatures (°C)		composition (wt %)					
	cellulose	PEO	water	protein	cellulose	PEO	ash	cellulose/PEO (w/w)
pure BC	346 ± 2		13 ± 4	14 ± 4	43 ± 11		30 ± 4	100:0
control PEO		410 ± 1				96 ± 1	4 ± 1	0:100
BC in 0.5% PEO	346 ± 7	426 ± 3	11 ± 6	11 ± 5	30 ± 5	21 ± 2	27 ± 2	59:41
BC in 1% PEO	351 ± 2	428 ± 4	12 ± 2	10 ± 5	27 ± 5	24 ± 3	28 ± 2	53:47
BC in 2% PEO	351 ± 2	429 ± 1	9 ± 1	10 ± 1	19 ± 3	39 ± 3	23 ± 2	33:67
BC in 3% PEO	352 ± 2	427 ± 2	9 ± 2	6 ± 4	15 ± 4	42 ± 11	27 ± 10	23:77
BC in 5% PEO	348 ± 4	425 ± 5	7 ± 1	6 ± 1	12 ± 6	50 ± 12	24 ± 7	15:85

Table 2. Thermal Transitions and Other Morphological Characteristics of PEO and BC in Nanocomposites of Varying BC/PEO Ratios[a]

	poly(ethylene oxide)			bacterial cellulose		
BC/PEO (w/w)	T_g (°C)	T_m (°C)	X_c	I_β/I_α	nanofiber width (nm)	bundles width (nm)
100:0				1.0 ± 0.1	17 ± 5	75−111
59:41	−50 ± 6	60 ± 1	0.21 ± 0.07			
53:47	−50 ± 4	62 ± 3	0.36 ± 0.22		10 ± 2	83−466
33:67	−48 ± 1	63 ± 1	0.49 ± 0.05			
23:77	−48 ± 3	66 ± 5		1.3 ± 0.2	10 ± 2	102−690
15:85	−51 ± 2	68 ± 3	0.49 ± 0.06	1.3 ± 0.2	10 ± 2	121−770
0:100	−52 ± 1	68 ± 1	0.67 ± 0.01			

[a] Blend characteristics after impurities were pyrolyzed.

medium during BC synthesis the dimensions of the cellulose nanofibers and of the characteristic aggregates can be tailored. They also confirm that this manufacturing approach allows PEO to intimately blend with cellulose whether it is a 10 nm wide cellulose nanofiber or 100−770 nm wide bundles of nanofibers. In other words, truly dispersed cellulose/PEO nanocomposites are manufactured. Clearly, by augmenting the culture medium with the desired matrix polymer, an excellent dispersion of high aspect ratio nanofibers can be achieved, circumventing the aggregation issue that is often encountered with other nanoscale reinforcements such as cellulose whiskers.[38,39] In essence, this integrated biomanufacturing approach therefore weaves the thermoplastic polymer in the cellulose nanofibers, thereby yielding nanocomposites with a remarkably fine morphology considering that the nanofibers have a high aspect ratio of around 1000.[30] To evaluate whether this manufacturing approach also could be used to tailor the composition of the cellulose/PEO nanocomposite, thermogramimetric analysis (TGA) was conducted.

Tailoring the Composition of Cellulose/PEO Nanocomposites. In Figure 3, the TGA traces for control PEO, neat BC, and one of the BC/PEO nanocomposites are shown along with the derivative traces. The derivative traces are best suited to determine the decomposition temperatures for each constituent, whereas the weight traces can be used to determine the weight loss associated with the decomposition of this constituent.[36] For PEO, a single degradation temperature was clearly observed at 410 ± 1 °C. For bacterial cellulose, decomposition involved three stages having peak temperatures at 159 ± 4, 218 ± 4, and 346 ± 2 °C. These three weight loss stages could be attributed to the loss of bound water, proteinaceous material from the bacterial cells, and cellulose, respectively.[40] In the washed native bacterial cellulose, the water content and proteinaceous content were measured at 13% ± 4% and 14% ± 4%, respectively (Table 1). These values are consistent with the amount of nonfreezing bound water associated with highly crystalline cellulose[41] and with the amount of proteins and nucleic acids that arise from bacterial cells in native cellulose,[40] supporting the fact that the washing procedure had effectively removed compounds other than the bacterial cells. In the BC/PEO nanocomposites, all four degradation temperatures were clearly observed, allowing for the calculation of the weight percent of bound water, proteinaceous material, cellulose, PEO, and ash (Figure 3). As expected, modification of the culture medium with various concentrations of PEO resulted in different TGA traces and therefore compositions (Figure 3). By increasing the PEO concentration in the HS medium from 0.5 to 5 wt %, the PEO content in the nanocomposite increased. In parallel with the reduction in the cellulose content, the contents in bound

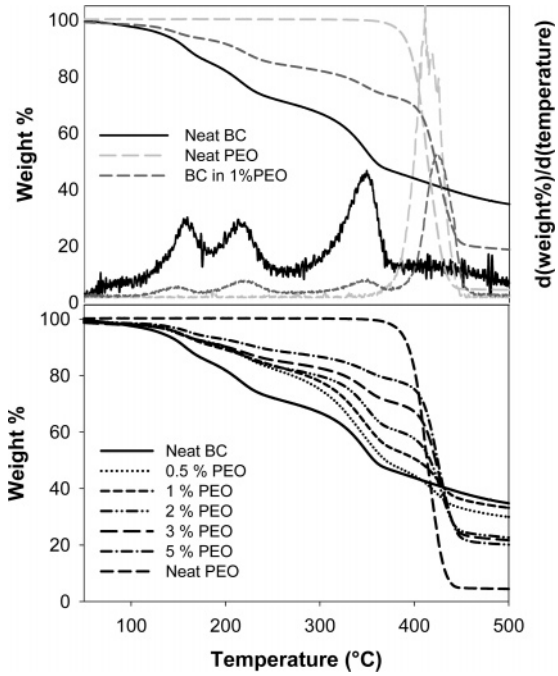

Figure 3. Thermogravimetric analysis illustrating the original and derivative curves for the neat BC and PEO (top) and for all the BC/PEO nanocomposites as a function of the culture medium modification (bottom).

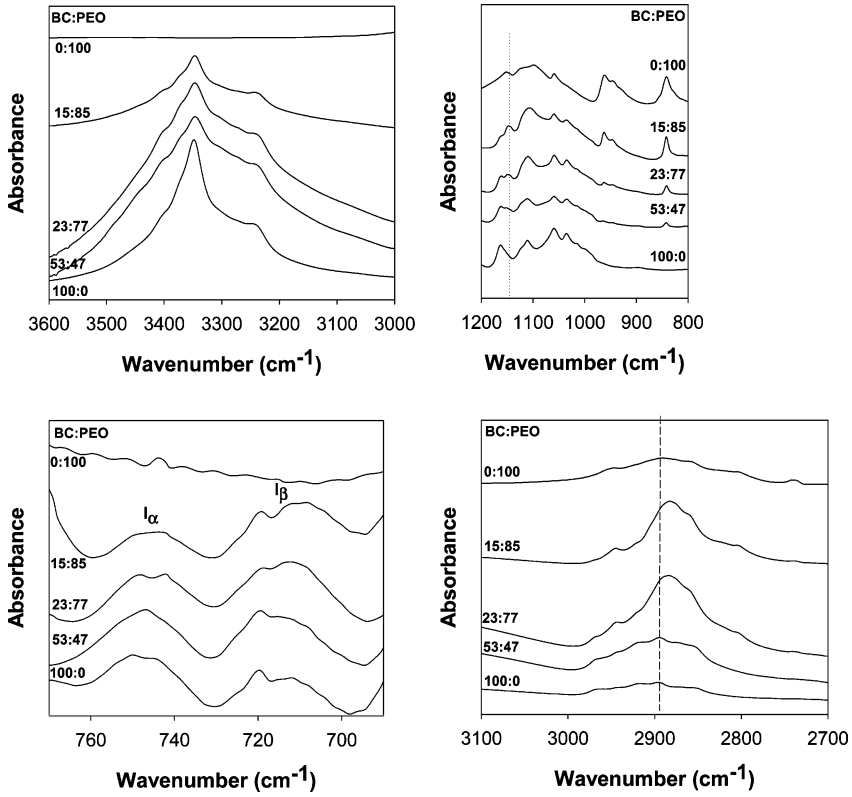

Figure 4. FTIR spectra of BC/PEO nanocomposites as a function of the BC/PEO w/w ratio.

water, proteinaceous material, and ash also decreased (Table 1). This is expected because the bound water is linked to the cellulose and the proteinaceous material relates to the bacteria cells. In fact, with the experimental conditions used in the study, the BC/PEO w/w ratio in the nanocomposites varied from 59:41 to 15:85, suggesting that any blend composition could be attained by appropriately modifying the culture medium (Table 1).

It is also interesting to note that the degradation temperatures of the PEO and the cellulose were increased by approximately 15 and 4 °C, respectively, in the nanocomposites compared to the control cellulose and PEO (Figure 3 and Table 1). Although small, this increase in degradation temperatures for both polymeric components was significant. It may be ascribed to mutual thermal stabilization as previously observed in blends of polystyrene and poly(vinyl chloride).[42] In polymer blends, mutual stabilization may arise from chemical interactions between the polymers and/or their decomposition products.[43] Thermal stabilization of PEO by cellulose is in contrast with previous observations on solvent cast cellulose whiskers/PEO,[44] possibly indicating enhanced dispersion and chemical interactions in the present biosynthetic approach or some contribution from the bacterial cell debris.

With the ability to tailor composition in the final nanocomposites, yields of glucose conversion into cellulose could be computed. The conversion yield of glucose into cellulose decreased from 32% in the standard HS medium to the 10−20% range with addition of PEO in the culture medium, possibly due to changes in viscosity with PEO addition.

The TGA results therefore confirm the hypothesis that the present manufacturing approach allows tailoring the composition of bacterial cellulose reinforced thermoplastic nanocomposites. Altogether, it is clear that composition, nanofiber dimensions, and dispersion in the polymer matrix can be tailored by manipulating the growth conditions of bacterial cellulose in a polymer matrix solution. This is likely true for PEO, because cellulose and PEO can develop favorable interactions.[32−34] To further assess the intermolecular interactions, miscibility, and thermal properties of the cellulose/PEO nanocomposites, FTIR spectroscopy and DSC measurements were evaluated.

Evaluation of Intermolecular Interactions and Crystallinity in BC/PEO Nanocomposites. Strong interactions between the primary hydroxyl group at the C_6 position of the glucose and the ether oxygen of the PEO have been previously observed in blends of cellulose and PEO.[32] However, hydrogen bonding between cellulose and PEO was not obvious in the FTIR spectra of the composite materials as the absorption band for the cellulosic hydroxyl at around 3350 cm^{-1} was unchanged by the presence of PEO (Figure 4). However, a new C−O−C stretching absorption band that was not apparent in either of the neat components was observed at 1148 cm^{-1} in the nanocomposites. Absorption at this wavelength indicated that the PEO C−O−C stretching was perturbed in the nanocomposites compared to the neat PEO state, possibly as a result of interactions, such as hydrogen bonding, between cellulose and PEO or as a result of a morphological change in PEO.[33]

Furthermore, there was a clear change in the crystallinity of both cellulose and PEO in the nanocomposites compared to their neat states. First, the CH_{2-} asymmetric stretching of PEO shifted from 2890 cm^{-1} for pure PEO to 2883 cm^{-1} in the BC/PEO composite, suggesting a decrease in PEO crystallinity (Figure 4).[45] The cellulose morphology was also altered, as demonstrated by the changes in the 750 and 710 cm^{-1} absorption bands that are characteristic of the I_α and I_β crystalline allomorphs, respectively.[26] As the PEO content increased in the composite, the I_β/I_α allomorph ratio, measured from the intensity ratio of the respective absorption bands, increased from 1.0 for neat bacterial cellulose to ca. 1.3 in the BC/PEO composites (Table 2). The presence of PEO in the culture medium therefore favored cellulose crystallization into the more stable I_β allomorph over

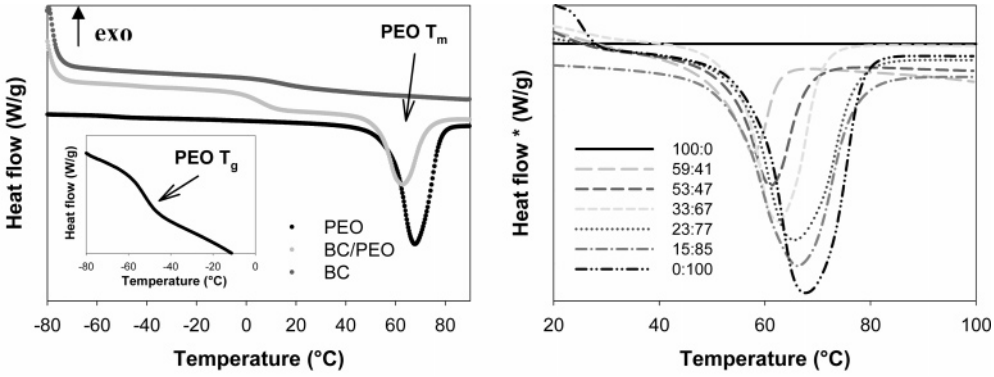

Figure 5. DSC thermograms illustrating the determination of the glass transition and melting temperatures in the nanocomposite (left) and the variation in the melting endotherm of PEO as a function of the BC/PEO w/w ratio (right).

the I_α allomorph as previously observed with other culture modifications. The increase in production of the I_β allomorph is consistent with the observed crystallization into finer nanofibers as PEO content increased.[26] The possibility that the bacterial cells remaining in the composite had caused the chemical changes observed in the FTIR spectra was also considered. Whole bacterial cells have dimensions in the 1−5 μm range, allowing little molecular contact with either PEO or cellulose, at least when compared to the scale of mixing that was previously observed between PEO and cellulose. Furthermore, the observed changes in the FTIR spectra were consistent with previous FTIR studies on pure PEO/cellulose blends, supporting that the changes observed in the FTIR spectra arose principally from cellulose/PEO miscibility.[33]

Nevertheless, to further evaluate miscibility between the constituents and thermal behavior, the main thermal transitions, glass transition temperatures (T_g) and melting temperatures (T_m), were evaluated and compared to those of the neat components. The DSC scans of the BC/PEO composites allowed determination of the T_g and the T_m of the PEO in the nanocomposites at around −50 and 60 °C, respectively (Figure 5). The crystallinity index of the PEO in the composite material was also computed from the heat of fusion using a ΔH_f for pure crystalline PEO of 201.2 J/g (Table 2).[46] The heat of fusion per gram of PEO was used so that the reported index is the crystallinity of PEO alone within the nanocomposite. The T_g of PEO was clearly detected for all nanocomposites at around −50 °C independently of composition (Table 2), suggesting that mixing was not occurring between the amorphous fraction of PEO and any other constituents.

In contrast, the T_m and heat of fusion of the PEO was greatly depressed by the presence of cellulose in the nanocomposites (Figure 5). In fact the depression of the PEO T_m by approximately 10 °C was accompanied by a large drop in crystallinity from about 67% to 21% (Table 2). The T_m and crystallinity index of PEO decreased proportionally to the cellulose content in the nanocomposite. These results are similar to those obtained on tunicin whiskers/PEO nanocomposites.[44] In tunicin whiskers/PEO composites, the T_g of PEO was unaffected by the addition of up to 30% cellulose whisker, whereas the T_m and crystallinity index of PEO were significantly depressed by the presence of cellulose. The diameter of the PEO spherulites was also found to decrease from approximately 200 to 10 μm with the addition of 10% cellulose whiskers. This behavior was ascribed to cellulose whiskers acting has a nucleating surface for PEO and also sterically hindering spherulitic growth due to their fine dispersion into the PEO.[44] Although the PEO was of higher molecular weight (1×10^6 g/mol) than in the present study, similar morphological effects

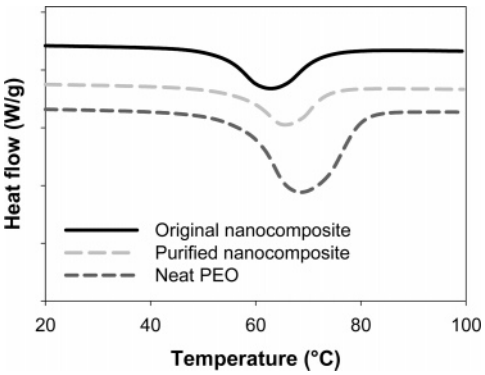

Figure 6. DSC thermograms illustrating the melting temperatures and heat of fusion of the neat PEO and the nanocomposite with a BC/PEO ratio of 53:47 before and after pyrolysis of the bacteria cell debris.

could have contributed to the depression in melting temperature and crystallinity in the BC/PEO nanocomposites. That is, in the presence of bacterial cellulose, PEO crystallization may have been hindered by the dispersion of cellulose nanofibers yielding smaller and less stable crystals. Depression in melting points is also consistent with the thermodynamic effects of miscibility between cellulose and PEO.[32,34] However in contrast to the FTIR analysis, during the DSC experiments the high temperature is likely to lyse the bacterial cell, resulting in the liberation of the phospholipids and nucleic acids from the cytoplasm and of the proteins, lipids, and carbohydrates from the cell envelope of the microorganism.[47,48] It is therefore possible that the bacteria cell debris also contributed to the depression in melting point and crystallinity of the PEO. To verify this possibility, a reference experiment was conducted on the nanocomposite grown in 1% w/w PEO, i.e., having a BC/PEO ratio of 53:47. In this reference experiment, the sample was heated to 250 °C and maintained at that temperature for 5 min, at which point 22% weight loss had occurred, ensuring that water and the proteinaceous material had evaporated and pyrolyzed respectively. After this thermal treatment, the T_m and crystallinity index of the PEO were determined following the same temperature schedule as that done on the reference cellulose/PEO nanocomposite. After removal of the impurities, the T_m of PEO was lower than that of the neat PEO but not as low as that measured in the original nanocomposite, indicating that both the cellulose and the bacteria cell debris participated in the melting point depression (Figure 6). In contrast, the crystallinity index in the purified nanocomposite was similar to that of the original nancomposite at 0.40 ± 0.03, supporting the premise that the cellulose alone hindered PEO crystallization due to its fine dispersion in the PEO matrix.

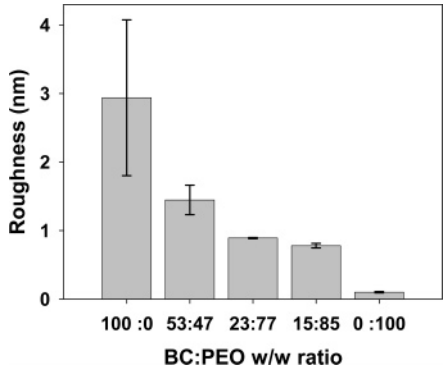

Figure 7. Root-mean-square roughness of the BC/PEO nanocomposites as a function of the BC/PEO w/w ratio.

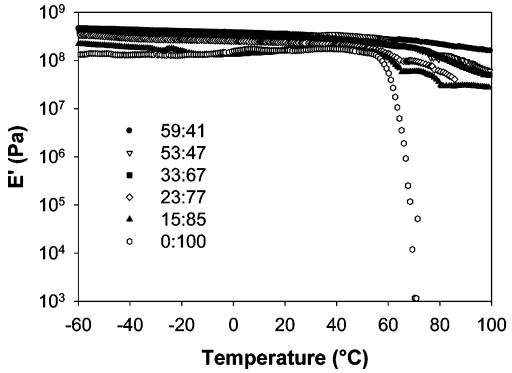

Figure 8. Storage tensile modulus E' versus temperature at 1 Hz for nanocomposites of varying BC/PEO w/w ratios.

Physical and Mechanical Properties of BC/PEO Nanocomposites. When grown under agitated conditions, pure bacterial cellulose dries in the form of clumps of disorganized fibrils that are easily torn apart. In contrast, the nanocomposites were in the form of fibrous material that could be easily molded into resilient and bendable films. The surface topography of the nanocomposites changed with composition. As the BC/PEO ratio decreased from 59:40 to 15:85, the nanocomposites became smoother with root-mean-square roughness dropping to the subnanometer level as measured by AFM (Figure 7). This indicated that in the nanocomposites the surface roughness may be tailored from composition, which may be of particular interest for biomaterial applications requiring specific surface properties and adhesion.

The linear mechanical behavior of the nanocomposites was also evaluated in tensile mode under dynamic loading (Figure 8). Note that the neat bacterial cellulose was not tested as the formed sheet was brittle and easily broken. The storage moduli of both pure PEO and cellulose/PEO nanocomposites decreased slightly from −70 to about 60 °C with no apparent T_g (Figure 8). Interestingly, the nanocomposites with higher BC content had a higher subambient modulus, although the differences were small. As the melting point of PEO approached at around 60 °C, the dramatic drop in E' that was observed in the control PEO was significantly reduced by the cellulose reinforcement. Again the modulus drop decreased with increasing cellulose content in the nanocomposites. At a BC/PEO ratio of 59:41 there was almost no noticeable drop in E' at the melting point of PEO. Clearly, cellulose provided significant thermal stabilization of the modulus of the PEO matrix above its melting point. A similar behavior has been observed in tunicin whiskers/PEO nanocomposites and was ascribed to the formation of a rigid percolating cellulose nanocrystals network.[49,50] The much greater aspect ratio of bacterial cellulose (1000) compared to that of tunicin nanocrystals (70) may further explain the large reinforcing effect in BC/PEO nanocomposites although again there may be some contribution from the bacterial cell debris. The lower crystallinity index in nanocomposites having higher cellulose content also likely contributed to the observed stabilization.

Conclusions

The potential of manipulating the biogenesis of bacterial cellulose to produce fiber-reinforced thermoplastic nanocomposites of controlled composition, morphology, and properties was demonstrated. By modifying the culture medium of bacterial cellulose with various concentrations of poly(ethylene oxide), nanocomposites were produced with BC/PEO w/w ratios ranging from 15:85 to 59:41. As the PEO content increased, the cellulose crystallized into smaller nanofibers (ca. 20 to 10 nm in width) that were finely dispersed into PEO. The nanofibers were further bonded together into bundles, 75−770 nm wide, that systematically widened as the PEO content increased. At the same time, the I_β cellulose allomorph became more prominent, and the crystallinity and melting temperature of PEO decreased. The observed morphological modifications of PEO were principally ascribed to the fine dispersion of cellulose nanofibers into the PEO matrix but also to intermolecular interactions such as hydrogen bonding as demonstrated by FTIR spectroscopy. The bacterial cell debris also contributed to the melting point depression.

Expectedly then, the thermal and mechanical properties of the nanocomposites depended on composition and morphology. The thermal decomposition temperature of PEO increased by 15 °C in the nanocomposites, and this increase was ascribed to mutual thermal stabilization with cellulose. When tested in tension, BC effectively reinforced the PEO matrix in the glassy and rubbery states and most significantly above the melting temperature of PEO. The reinforcing effect was proportional to the cellulose content. Surface roughness was also significantly reduced with increasing PEO content.

This research therefore demonstrates the potential to biologically engineer phase morphology and selected physical, thermal, and mechanical properties in fiber-reinforced thermoplastic nanocomposites. Future research steps could involve the removal of the bacterial cell debris or the processing and utilization of the nanocomposites as produced. Indeed, the observed property enhancement in these nanoomposites compared to neat PEO pose the question of the necessity to remove bacterial cell debris in biologically produced materials for a specific application.

Acknowledgment. This research was partly supported by the International Marketing Program for Agricultural Commodities and Trade Center at Washington State University. E.E.B. thanks the Society of Women Engineers for her fellowship. The authors are also grateful to Professor Candace Haigler for sharing her experience in the synthesis of bacterial cellulose in modified agitated media. Finally, we thank the reviewers for their useful comments.

References and Notes

(1) Jonas, R.; Farah, L. F. Production and application of microbial cellulose. *Polym. Degrad. Stab.* **1998**, *59*, 101−106.
(2) Miranda, B. T.; Miranda, S. R.; Chan, L. P.; Saqueton, E. R. Some studies on nata. *Nat. Appl. Sci. Bull.* **1965**, *19* (1), 67−79.
(3) Nishi, Y.; Uryu, M.; Yamanaka, S.; Watanabe, K.; Kitamura, N.; Iguchi, M.; Mitsuhashi, S. The structure and mechanical properties of sheets prepared from bacterial cellulose. 2. Improvement of the mechanical properties of sheets and their applicability to diaphragms of electroacoustic transducers. *J. Mater. Sci.* **1990**, *25* (6), 2997−3001.

(4) Shah, J.; Brown, R. M. Towards electronic paper displays made from microbial cellulose. *Appl. Microbiol. Biotechnol.* **2005**, *66* (4), 352−355.

(5) Yano, H.; Sugiyama, J.; Nakagaito, A. N.; Nogi, M.; Matsuura, T.; Hikita, M.; Handa, K. Optically transparent composites reinforced with networks of bacterial nanofibers. *Adv. Mater.* **2005**, *17* (2), 153−5.

(6) Czaja, W. K.; Young, D. J.; Kawecki, M.; Brown, R. M. The future prospects of microbial cellulose in biomedical applications. *Biomacromolecules* **2007**, *8* (1), 1−12.

(7) Ciechanska, D.; Struszczyk, H.; Guzinska, K. Modification of bacterial cellulose. *Fibres Text. East. Eur.* **1998**, *6* (4), 61−65.

(8) Czaja, W.; Krystynowicz, A.; Bielecki, S.; Brown, R. M. Microbial cellulose—The natural power to heal wounds. *Biomaterials* **2006**, *27* (2), 145−151.

(9) Legeza, V. I.; Galenko-Yaroshevskii, V. P.; Zinov'ev, E. V.; Paramonov, B. A.; Kreichman, G. S.; Turkovskii, I. I.; Gumenyuk, E. S.; Karnovich, A. G.; Khripunov, A. K. Effects of new wound dressings on healing of thermal burns of the skin in acute radiation disease. *Bull. Exp. Biol. Med.* **2004**, *138* (3), 311−315.

(10) Klemm, D.; Schumann, D.; Udhardt, U.; Marsch, S. Bacterial synthesized cellulose—Artificial blood vessels for microsurgery. *Prog. Polym. Sci.* **2001**, *26* (9), 1561−1603.

(11) Klemm, D.; Udhardt, U.; Marsch, S.; Schumann, D. I. Cellulose. BASYC, Bacterially synthesized cellulose. Miniaturized tubes for microsurgery. *Polym. News* **1999**, *24* (11), 377−378.

(12) Backdahl, H.; Helenius, G.; Bodin, A.; Nannmark, U.; Johansson, B. R.; Risberg, B.; Gatenholm, P. Mechanical properties of bacterial cellulose and interactions with smooth muscle cells. *Biomaterials* **2006**, *27* (9), 2141−2149.

(13) Helenius, G.; Backdahl, H.; Bodin, A.; Nannmark, U.; Gatenholm, P.; Risberg, B. In vivo biocompatibility of bacterial cellulose. *J. Biomed. Mater. Res., Part A* **2006**, *76* (2), 431−438.

(14) Svensson, A.; Nicklasson, E.; Harrah, T.; Panilaitis, B.; Kaplan, D. L.; Brittberg, M.; Gatenholm, P. Bacterial cellulose as a potential scaffold for tissue engineering of cartilage. *Biomaterials* **2005**, *26*, 419−431.

(15) Watanabe, K.; Eto, Y.; Takano, S.; Nakamori, S.; Shibai, H.; Yamanaka, S. A new bacterial cellulose substrate for mammalian cell culture—A new bacterial cellulose substrate. *Cytotechnology* **1993**, *13* (2), 107−114.

(16) Guilak, F.; Butler, D. L.; Goldstein, S. A.; Mooney, D. J. *Functional Tissue Engineering*; Springer: New York, 2003; p 426.

(17) Hong, L.; Wang, Y. L.; Jia, S. R.; Huang, Y.; Gao, C.; Wan, Y. Z. Hydroxyapatite/bacterial cellulose composites synthesized via a biomimetic route. *Mater. Lett.* **2006**, *60* (13−14), 1710−1713.

(18) Wan, Y. Z.; Hong, L.; Jia, S. R.; Huang, Y.; Zhu, Y.; Wang, Y. L.; Jiang, H. J. Synthesis and characterization of hydroxyapatite−bacterial cellulose nanocomposites. *Compos. Sci. Technol.* **2006**, *66* (11−12), 1825−1832.

(19) Yasuda, K.; Gong, J. P.; Katsuyama, Y.; Nakayama, A.; Tanabe, Y.; Kondo, E.; Ueno, M.; Osada, Y. Biomechanical properties of high-toughness double network hydrogels. *Biomaterials* **2005**, *26* (21), 4468−4475.

(20) Millon, L. E.; Mohammadi, H.; Wan, W. K. Anisotropic polyvinyl alcohol hydrogel for cardiovascular applications. *J. Biomed. Mater. Res., Part B* **2006**, *79* (2), 305−311.

(21) Ciechanska, D. Multifunctional bacterial cellulose/chitosan composite materials for medical applications. *Fibres Text. East. Eur.* **2004**, *12* (4), 69−72.

(22) Seifert, M.; Hesse, S.; Kabrelian, V.; Klemm, D. Controlling the water content of never dried and reswollen bacterial cellulose by the addition of water-soluble polymers to the culture medium. *J. Polym. Sci., Part A: Polym. Chem.* **2004**, *42* (3), 463−470.

(23) Haigler, C. H.; White, A. R.; Brown, R. M. J.; Cooper, K. M. Alteration of in vivo cellulose ribbon assembly by carboxymethylcellulose and other cellulose derivatives. *J. Cell Biol.* **1982**, *94* (1), 64−69.

(24) Hirai, A.; Tsuji, M.; Yamamoto, H.; Horii, F. In situ crystallization of bacterial cellulose III. Influences of different polymeric additives on the formation of microfibrils as revealed by transmission electron microscopy. *Cellulose* **1998**, *5* (3), 201−213.

(25) Uhlin, K. I.; Atalla, R. H.; Thompson, N. S. Influence of hemicelluloses on the aggregation patterns of bacterial cellulose. *Cellulose* **1995**, *2* (2), 129−144.

(26) Yamamoto, H.; Horii, F.; Hirai, A. In situ crystallization of bacterial cellulose. II. Influences of different polymeric additives on the formation of celluloses I_α and I_β at the early stage of incubation. *Cellulose* **1996**, *3* (1), 229−242.

(27) Brown, R. M. J.; Willison, J. H.; Richardson, C. L. Cellulose biosynthesis in *Acetobacter xylinum*: Visualization of the site of synthesis and direct measurement of the in vivo process. *Proc. Natl. Acad. Sci. U.S.A.* **1976**, *73* (12), 4565−4569.

(28) Haigler, C. H.; Brown, R. M. J.; Benziman, M. Calcofluor white ST alters the in vivo assembly of cellulose microfibrils. *Science* **1980**, *210* (4472), 903−906.

(29) Yamanaka, S.; Ishihara, M.; Sugiyama, J. Structural modification of bacterial cellulose. *Cellulose* **2000**, *7* (3), 213−225.

(30) Zaar, K. The biogenesis of cellulose by *Acetobacter xylinum*. *Cytobiologie* **1977**, *16* (1), 1−15.

(31) Seal, B. L.; Otero, T. C.; Panitch, A. Polymeric biomaterials for tissue and organ regeneration. *Mater. Sci. Eng., R* **2001**, *34* (4−5), 147−230.

(32) Kondo, T.; Sawatari, C. Intermolecular hydrogen-bonding in cellulose poly(ethylene oxide) blends: Thermodynamic examination using 2,3-di-*O*- and 6-*O*-methylcelluloses as cellulose model compounds. *Polymer* **1994**, *35* (20), 4423−4428.

(33) Kondo, T.; Sawatari, C.; Manley, R. S.; Gray, D. G. Characterization of hydrogen-bonding in cellulose−synthetic polymer blend systems with regioselectively substituted methylcellulose. *Macromolecules* **1994**, *27* (1), 210−215.

(34) Nishio, Y.; Hirose, N.; Takahashi, T. Thermal analysis of cellulose/poly(ethylene oxide) blends. *Polym. J.* **1989**, *21* (4), 347−351.

(35) Hestrin, S.; Schramm, M. Synthesis of cellulose by *Acetobacter xylinum*. II. Preparation of freeze-dried cells capable of polymerizing glucose to cellulose. *Biochem. J.* **1954**, *58* (2), 345−352.

(36) American Society for Testing Materials. *Standard Test Method for Compositional Analysis by Thermogravimetry*; ASTM E1131-03; American Society for Testing Materials: Philadelphia, PA, 2003; Vol. 14.02.

(37) Brown, R. M. J. The biosynthesis of cellulose. *J. Macromol. Sci., Pure Appl. Chem.* **1996**, *33* (10), 1345−1373.

(38) Azizi Samir, M. A. S.; Alloin, F.; Sanchez, J. Y.; El Kissi, N.; Dufresne, A. Preparation of cellulose whiskers reinforced nanocomposites from an organic medium suspension. *Macromolecules* **2004**, *37* (4), 1386−1393.

(39) Ljungberg, N.; Bonini, C.; Bortolussi, F.; Boisson, C.; Heux, L.; Cavaillé, J. Y. New nanocomposite materials reinforced with cellulose whiskers in atactic polypropylene: Effect of surface and dispersion characteristics. *Biomacromolecules* **2005**, *6* (5), 2732−2739.

(40) George, J.; Ramana, K. V.; Sabapathy, S. N.; Jagannath, J. H.; Bawa, A. S. Characterization of chemically treated bacterial (*Acetobacter xylinum*) biopolymer: Some thermo-mechanical properties. *Int. J. Biol. Macromol.* **2005**, *37* (4), 189−194.

(41) Nakamura, K.; Hatakeyama, T.; Hatakeyama, H. Effect of bound water on tensile properties of native cellulose. *Text. Res. J.* **1983**, *53* (11), 682−688.

(42) Dodson, B.; McNeill, I. C. Degradation of polymer mixtures. IV. Blends of poly(vinyl chloride) with polystyrene. *J. Polym. Sci. Part A: Polym. Chem.* **1976**, *14* (2), 353−364.

(43) *Thermal Characterization of Polymeric Materials*, 2nd ed.; Turi, E. A., Ed.; Academic Press: San Diego, CA, 1997.

(44) Azizi Samir, M. A. S.; Alloin, F.; Sanchez, J. Y.; Dufresne, A. Cellulose nanocrystals reinforced poly(oxyethylene). *Polymer* **2004**, *45* (12), 4149−4157.

(45) Bailey, F. E., Jr.; Koleske, J. V. *Poly(ethylene oxide)*; Academic Press: New York, 1976; p 173.

(46) *Polymer Data Handbook*; Mark, J. E., Ed.; Oxford University Press: New York, 1999; p 1018.

(47) Ede, S. M.; Hafner, L. M.; Fredericks, P. M. Structural changes in the cells of some bacteria during population growth: A Fourier transform infrared-attenuated total reflectance study. *Appl. Spectrosc.* **2004**, *58* (3), 317−322.

(48) Yu, C. X.; Irudayaraj, J. Spectroscopic characterization of microorganisms by Fourier transform infrared microspectroscopy. *Biopolymers* **2005**, *77* (6), 368−377.

(49) Schroers, M.; Kokil, A.; Weder, C. Solid polymer electrolytes based on nanocomposites of ethylene oxide−epichlorohydrin copolymers and cellulose whiskers. *J. Appl. Polym. Sci.* **2004**, *93* (6), 2883−2888.

(50) Azizi Samir, M. A. S.; Chazeau, L.; Alloin, F.; Cavaillé, J. Y.; Dufresne, A.; Sanchez, J. Y. POE-based nanocomposite polymer electrolytes reinforced with cellulose whiskers. *Electrochim. Acta* **2005**, *50* (19), 3897−3903.

BM700448X